Published in final edited form as:
*Cancer Res*. 2020 June 15; 80(12): 2586–2598. doi:10.1158/0008-5472.CAN-19-2660.

# Tumor cell-derived Angiopoietin-2 promotes metastasis in melanoma

**Ashik Ahmed Abdul Pari**[1,2,*], **Mahak Singhal**[1,2,*], **Corinne Hübers**[2,3], **Carolin Mogler**[5], **Benjamin Schieb**[1,2], **Anja Gampp**[1,2], **Nicolas Gengenbacher**[1,2], **Louise E. Reynolds**[6], **Dorothee Terhardt**[2], **Cyrill Géraud**[1,3,4], **Jochen Utikal**[3,7], **Markus Thomas**[8], **Sergij Goerdt**[1,3], **Kairbaan Hodivala-Dilke**[6], **Dr. Hellmut G. Augustin**[1,2,9,#], **Dr. Moritz Felcht**[1,3,#]

[1]European Center for Angioscience (ECAS), Medical Faculty Mannheim, Heidelberg University, Mannheim, Germany

[2]Vascular Oncology and Metastasis, German Cancer Research Center, Heidelberg (DKFZ-ZMBH Alliance), Germany

[3]Department of Dermatology, Venerology und Allergology, University Medical Center Mannheim, Medical Faculty Mannheim, Heidelberg University, Mannheim, Germany

[4]Section of Clinical and Molecular Dermatology, Medical Faculty Mannheim, Heidelberg University, Mannheim, Germany

[5]Institute of Pathology, Technical University of Munich, Munich, Germany

[6]Center for Tumour Biology, Barts Cancer Institute, Queen Mary University of London, John Vane Science Center, London, United Kingdom

[7]Skin Cancer Unit, German Cancer Research Center (DKFZ), Heidelberg, Germany

[8]Roche Pharma Research and Early Development, Roche Innovation Center Munich, Roche Diagnostics GmbH, Penzberg, Germany

[9]German Cancer consortium, Heidelberg, Germany

## Abstract

The Angiopoietin (Angpt)-TIE signaling pathway controls vascular maturation and maintains the quiescent phenotype of resting vasculature. The contextual agonistic and antagonistic Tie2 ligand ANGPT2 is believed to be exclusively produced by endothelial cells, disrupting constitutive ANGPT1-TIE2 signaling to destabilize the microvasculature during pathological disorders like inflammation and cancer. However, scattered reports have also portrayed tumor cells as a source of ANGPT2. Employing in situ hybridization-based detection of *ANGPT2*, we found strong tumor

Correspondence to: Hellmut G. Augustin; Moritz Felcht.

**Corresponding authors:** Dr. Moritz Felcht European Center for Angioscience, Medical Faculty Mannheim, Heidelberg University, and Department of Dermatology, Venerology and Allergy Theodor-Kutzer-Ufer 1-3, D-68167 Mannheim, Germany, Phone: +48-621-383-2280, Moritz.felcht@umm.de Dr. Hellmut G. Augustin European Center for Angioscience, Medical Faculty Mannheim, Heidelberg University, and German Cancer Research Center Heidelberg Im Neuenheimer Feld 280, D-69120 Heidelberg, Germany, Phone: +49-6221-421500, augustin@angiogenese.de.
[*]equally contributing first authors
[#]equally contributing last authors

**Conflict of interest:** Markus Thomas is an employee of Roche.


Europe PMC Funders Author Manuscripts

cell expression of *ANGPT2* in a subset of melanoma patients. Comparative analysis of biopsies revealed a higher fraction of *ANGPT2*-expressing tumor cells in metastatic versus primary sites. Tumor cell-expressed *Angpt2* was dispensable for primary tumor growth, yet in-depth analysis of primary tumors revealed enhanced intratumoral necrosis upon silencing of tumor cell *Angpt2* expression in the absence of significant immune and vascular alterations. Global transcriptional profiling of *Angpt2*-deficient tumor cells identified perturbations in redox homeostasis and an increased response to cellular oxidative stress. Ultrastructural analyses illustrated a significant increase of dysfunctional mitochondria in *Angpt2*-silenced tumor cells, thereby resulting in enhanced ROS production and downstream MAPK stress signaling. Functionally, enhanced ROS in *Angpt2*-silenced tumor cells reduced colonization potential in vitro and in vivo. Taken together, these findings uncover the hitherto unappreciated role of tumor cell-expressed ANGPT2 as an autocrine positive regulator of metastatic colonization and validate ANGPT2 as a therapeutic target for a well-defined subset of melanoma patients.

### Keywords

Angiopoietin-2; melanoma; metastasis; ROS; mitochondria; necrosis

## Introduction

Melanoma patients with the occurrence of metastases at distant sites exhibit a modest 5-year survival rate of 23%, making metastasis the leading cause of melanoma-associated death (1). Recent advances in the development of novel targeted therapies against receptor tyrosine kinases (BRAF and MEK1/2) and immune checkpoints (PD-1, PD-L1, and CTLA-4) have significantly improved the overall survival and long-term disease containment for melanoma patients. Yet, only a fraction of patients with metastatic disease show long-term responses to these treatments while a majority will develop resistance towards these therapies (2,3). Furthermore, melanoma metastases can occur in the absence of any apparent primary tumor, indicating that tumor cell dissemination and metastatic seeding are early and parallel events to primary tumor progression (2,4). It is therefore necessary to unravel the underlying molecular mechanisms governing metastatic progression to rationally develop innovative strategies to treat metastatic melanoma.

Angiopoietin-2, a contextual agonistic and antagonistic ligand of the constitutive quiescence-maintaining endothelial ANGPT1/TIE2 signaling axis has in recent years intensely been pursued as a second-generation anti-angiogenic candidate molecule (5). Preclinically, genetic deletion of *Angpt2* resulted in a transient delay of primary tumor growth (6). Postsurgical adjuvant administration of an ANGPT2-neutralizing antibody in combination with low-dose metronomic chemotherapy restricted metastasis by quenching not only the angiogenic but also the inflammatory response of EC within the metastatic niche (7). In melanoma patients, circulating levels of ANGPT2 were associated with the progression of metastatic disease. Intriguingly, serum ANGPT2 levels were found significantly elevated in stage III/IV (metastases-bearing) but not in stage I/II (confined to the local site) melanoma patients as compared with healthy volunteers (8). These preclinical and clinical data have solidly established a crucial role of ANGPT2 during metastasis

progression, particularly of melanoma metastasis, one of the earliest metastasizing tumor entities (2,4).

ANGPT2 is an almost endothelial cell-specifically expressed cytokine that acts in an autocrine manner to promote vascular remodeling (9). However, few scattered publications have also reported low levels of ANGPT2 expression by tumor cells of different cancer entities (8,10–12). ANGPT2 is a secreted cytokine. Immunohistochemical analysis of tumor tissue sections therefore often results in a diffuse pattern of ANGPT2 expression, making it difficult to nearly impossible to accurately determine the cellular origin of secreted ANGPT2. Therefore, definite tracing of ANGPT2 expression within the tumor microenvironment will improve our current understanding of the relative contribution of tumor cell- versus EC-secreted ANGPT2 and will allow to study the functional contribution of tumor cell-secreted ANGPT2 for tumor progression and metastasis.

Employing *in situ* hybridization-based detection of *ANGPT2* mRNA, we unambiguously detected *ANGPT2* expression in a subset of human melanoma specimens. Indeed, a higher fraction of metastatic melanoma patients expressed *ANGPT2* in tumor cells when compared with the primary tumor and benign nevi patients. Based on these findings, we hypothesized that tumor cell-secreted ANGPT2 may contribute towards tumor progression and metastasis, possibly by affecting vascular functions or by acting in an autocrine manner on tumor cells. Detailed experimental analyses revealed that vascular or immune cell functions were not affected by tumor cell-secreted ANGPT2. Instead, tumor cell-derived ANGPT2 controlled metabolic functions of tumor cells and thereby promoted their metastatic colonization potential.

## Materials and Methods

### Cells

Murine MT-RET (RET) melanoma cell line was established by isolating and culturing tumor cells from a spontaneously developed tumor in MT-RET transgenic mice (13). LLC were obtained from ATCC. B16F10-Luc2 cells were purchased from Caliper life sciences, U.S.A. All human melanoma cells (SKMEL-173, SKMEL-28, C-32, WM266-4, A375, M37, SKMEL-147, and SKMEL-23) were kindly provided by J. Utikal. All cancer cells were cultured in DMEM high glucose (Gibco) supplemented with 10% FCS, 1% penicillin/streptomycin (Sigma) and 1x non-essential amino acid (Gibco). Human umbilical vein endothelial cells (HUVEC; Promocell) were cultured in Endopan-3 medium supplemented with growth factors (PAN Biotech GmbH). Mouse lung endothelial cells were acquired from Cell Biologics and were cultured in complete EC media (Cell Biologics). The cell lines used in this study were routinely tested for mycoplasma by PCR. RET and B16F10-Luc2 cells were transduced with lentiviral particles expressing shRNA constructs (Dharmacon): non-targeting (RHS4346), sh-1 *Angpt2* (V2LMM_74366) and sh-2 *Angpt2* (V2LMM_68229). LLC cells were transduced with lentivirus to overexpress either *Angpt2* or control Plenti vector. Control or *Angpt2*-silenced RET cells were transduced with lentivirus to overexpress either *Angpt2* or control Plenti vector for rescuing *Angpt2* downregulation.

### Antibodies

For immunofluorescence staining, primary [rat anti-CD31 (BD Bioscience, #550300), rabbit anti-ki67 (Bethyl Laboratories, #IHC-00375), rabbit anti-desmin (Abcam, #Ab15200-1)] and secondary [anti-rat Alexa488, anti-rabbit Alexa546 (Life Technologies)] were used. Nuclei were stained with Hoechst (Sigma).

For Western blot analyses, primary [pERK (Cell Signaling, #4370), ERK (Santa Cruz, #sc-94), (pP38 (Cell Signaling, #9215), p38 (Cell Signaling, #9228), and β-actin (Santa Cruz, #sc-1616-R)] and secondary [horseradish peroxidase-conjugated antibodies (Dako)] were used. Proteins were detected with ECL (Pierce) and viewed using Amersham imager 600 (GE).

### *In vivo* studies

Female C57BL/6N (WT) mice (8-10 weeks old) were purchased from Charles River. All mice were housed in a 12h light/dark cycle with free access to food and drinking water in specific pathogen-free animal facilities. All animal experiments were approved by the governmental (G257/18, G163/16 and G254/18 from Regierungspräsidium Karlsruhe, Germany) Animal Care and Use Committees.

For primary tumor experiments, mice were subcutaneously injected with $1x10^6$ control or *Angpt2*-silenced RET or B16F10 cells. Two weeks post tumor implantation, mice were sacrificed and tumors and blood samples were collected for further processing. For N-acetyl-L-cysteine (NAC) (Sigma, 616-91-1) experiments, treatment was initiated on the day of tumor injection. The mice received drinking water supplemented with NAC (1g/l).

For LLC tumor experiments, $1x10^6$ LLC Plenti or LLC Plenti-*Angpt2* cells were inoculated subcutaneously in C57BL/6N mice. Primary tumors were surgically resected at an average size of 150 $mm^3$. Mice were post-resection routinely checked for the experimental endpoint criteria.

For experimental metastasis, $2.5x10^5$ control or *Angpt2*-silenced RET or B16F10 cells were injected in the tail vein of 8-10 weeks old female WT mice. Mice were sacrificed 2 weeks after tumor cell inoculation. Lungs were harvested and the number of metastases were counted under a stereomicroscope. For NAC treatment, the treatment was initiated one day prior to tail vein injection. The mice either received regular drinking water or drinking water supplemented with NAC (1g/l).

For ear tumor model, $3x10^5$ (in 10 μl) control or *Angpt2*-silenced RET cells were injected in the ear dermis of 8-10 weeks old WT mice. Mice were sacrificed 2 weeks after tumor cell inoculation. Cervical LN were harvested and the incidence of melanoma metastasis was evaluated under a stereo-microscope.

For *in vivo* lung colonization assays, $1.5x10^5$ control (red) and *Angpt2*-silenced (green) cells were co-injected intravenously in the tail vein of 8-10 weeks old female WT mice. After 2 weeks, mice were sacrificed and lungs were harvested. Images of the harvested lungs were

taken using a stereomicroscope with fluorescence detection capabilities. Total RFP and GFP area in the lungs were calculated using Image J software.

### Patient samples

Tissue microarrays (TMA) were kindly generated by the tissue bank of the National Center for Tumor Diseases (NCT, Heidelberg, Germany) using the paraffin-embedded human tumor specimens.

### Ethical approval

The study was performed with archived paraffin-embedded tissue samples. The study was approved by the ethical committee of Heidelberg University (2014-835R-MA).

### Immunofluorescence and immunohistochemistry

Fresh tissue samples were embedded in Tissue-Tek OCT and cut into 7μm thick cryosections for IF staining. Images were acquired using Zeiss Axio Scan and image analysis was performed with Fiji.

For immunohistochemistry, tissue samples were fixed in Zinc-fixative and were embedded in paraffin. 7μm sections were cut and stained with Hematoxylin and Eosin. For necrosis analysis, tumor sections were analyzed by a board-certified pathologist (C. Mogler).

ANGPT2 staining was performed as described earlier (14). In brief, freshly-cut TMA sections were mounted on super frost glass plates and stained with anti-ANGPT2 antibody (Santa Cruz Biotechnology) using Ultraview universal HRP multimer detection kit (Ventana, USA). Tumor sections were analyzed by C. Mogler.

### *In situ* hybridization

*In situ* hybridization was performed on TMAs using a specific probe against human *ANGPT*2 and RNAscope®2.5 HD-Red kit (ACD, USA), according to the manufacturer's instructions. Afterward, the TMAs were counterstained with hematoxylin. Tumor sections were analyzed by C. Mogler.

### Anoikis assay

Tumor cells were cultured under suspension condition using ultra-low attachment plates (Costar, #CLS3471-24EA) for 48h. Thereafter, the fraction of apoptotic cells was determined by FACS-based quantitation of Annexin-V (eBioscience, #88-8007-74) and FxCycle (Invitrogen, #F10347) staining.

### Colony formation assay

Cells were cultured under anoikis conditions for 48h. Thereafter, 600 cells were seeded in a new 6-well plate and allowed to form colonies for 1wk. Colonies were fixed and stained with crystal violet. The number of colonies was counted manually.




Europe PMC Funders Author Manuscripts

### MTT proliferation assay

Cells (5,000) were seeded in a 96-well plate and allowed to adhere and grow for 48h. Cellular proliferation was analyzed using cell proliferation kit (Roche, #11465007001), according to manufacturer's instruction.

### Cell adhesion assay

HUVECs ($2.5x10^5$) were seeded in a 6-well plate to form a monolayer (24h). GFP-labeled tumor cells ($5x10^5$) in Opti-MEM media (Life Technologies) were seeded on the top of endothelial monolayer and allowed to adhere for 40min. Non-adherent tumor cells were washed with PBS and the count of adherent tumor cells was determined using BD CantoII.

### Adhesion assay

96-well plates were either coated with fibronectin 10μg/ml (Sigma) or Collagen-IV 10μg/ml (Sigma) at 4°C overnight or 1h at 37°C. Subsequently, 30,000 tumor cells in 100μl Opti-MEM media were seeded in octuplicates. The cells were allowed to adhere for 40min at 37°C. Non-adherent cells were removed by washing the plates with PBS. The adherent cells were stained with 0.1% crystal violet solution for 10min at RT. Next, crystal violet stain was solubilized in 100μl of methanol and measured at 550nm in a spectrophotometer.

### Cell migration assay

A CIM plate 16 (Roche Applied Science; 8 μm pore size) was used to measure tumor cell migration on a xCELLigence system (Roche). The lower wells of the CIM plate were filled with 160 μl full media and 100 μl serum free DMEM media was added on the upper wells. The plate was equilibrated for 1h at 37°C. After background measurement, 30,000 tumor cells in 30 μl serum free DMEM media were added to the upper chamber and the CIM plate was assembled onto the xCELLigence system and placed in the incubator at 37°C. Cell migration was assessed by monitoring changes in electric impedance every 15 min for 48h. The changes in cell index over time determined the slope of the real time impedance curve.

### Cell invasion assay

Cell invasion was evaluated using BD BioCoat™Matrigel™ invasion chamber (24 well plate, 8 mm pore size). After pre-hydration of invasion chambers for 1h, $2.5\times10^5$ tumor cells in 500 μL serum free DMEM were placed in the upper chamber and 750 μL of DMEM with 10% FBS was added into the lower chamber. After 24h incubation at 37°C, chambers were washed with PBS and fixed in Roti-Histofix (4% PFA) for 10 min. Invaded cells were stained with 0.1% crystal violet solution and counted by a bright field microscope.

### Transmigration assay

HUVEC ($1\times10^5$) were plated in the top chamber of 6.5-mm/8.0-μm 0.2% gelatin-coated Transwells (Corning) overnight. Thereafter, PKH 26-labeled tumor cells ($1\times10^5$) were seeded in the top chamber in serum free DMEM with DMEM containing 10% FCS also in the bottom chamber. Transwells were washed 8 h later and fixed with Roti-Histofix (4% PFA) for 10 min. Transmigrated PKH 26-labelled tumor cells were counted under a fluorescence microscope.

### Immune analysis

Primary tumors were digested using Liberase (Roche) mix in DMEM media at 37°C for 30 min. Following ACK-lysis, single-cell suspension was equally divided, and stained for either lymphoid [CD45-PacOrange (Life Technologies, #MCD4530), CD3e-APC-e780 (eBioscience, #47-0032), CD45R(B220)-PE-Cy7 (eBioscience, #25-0452), CD4-APC (BioLegend, #100412), CD8-PE (BD Pharmingen, #553033), and NK-1.1-PerCP-Cy5.5 (BioLegend, #108728)] or myeloid [CD45-PacOrange (Life Technologies, #MCD4530), CD11b-PE-Cy7 (eBioscience, #25-0112), F4/80-PE (BioLegend, #123110), Ly6C-APC-e780 (BioLegend, #128025), and Ly6G-APC (BioLegend, #127613)] panel. FxCycle-violet and 20μl CountBright™ Absolute Counting Beads (Thermo Fisher Scientific, #C36950) were added to exclude dead cells and to analyze the absolute cell numbers per mg of tissue, respectively. Samples were acquired on BD Aria FusionII and were analyzed with FlowJo software.

### ROS analysis

*In vivo*: Tumor tissues were processed into a single-cell suspension as described above and incubated with CellRox-Deep Red (Thermo Scientific, #C10422) for 30min at 37°C in full media (FM). Cellular ROS was measured by quantifying the mean fluorescent intensity (MFI) of CellROX dye in $FxCycle^{-}CD45^{-}CD31^{-}Ter119^{-}GFP^{+}$ tumor cells using BD CantoII.

*In vitro*: Cells were cultured in either FM or serum-starved media and kept under anoikis conditions for 48h. Thereafter, cells were stained with CellRox-Deep Red as described above. Live cells were analyzed for MFI of CellRox dye.

### ELISA

ANGPT2 protein levels in the cell culture supernatant and serum were determined using either mouse ANGPT2 (R&D, #MANG20) or human ANGPT2 (R&D, #DANG20) ELISA kits, according to the manufacturer's protocol.

### Gene expression analysis

Total RNA, isolated by homogenizing tumor tissue, was used for reverse transcription using QuantiTect Reverse Transcription Kit (Qiagen) according to the manufacturer's instructions. cDNA was used for RT-qPCR using TaqMan Fast Advanced Mastermix and TaqMan probes [*TEK* (Hs00945146_m1); *ANGPT2* (Hs01048042_m1); *ACTB* (Hs01060665_g1); *Angpt2* (Mm00545822_m1); *Hmox1* (Mm00516005_m1); *Actb* (Mm00607939-s1); *MKi67* (Mm01278617_m1); *Fis1* (Mm00481580_01); *Dnm1l* (Mm01342903_m1); Applied Biosystems] on a LightCycler-480 (Roche) system. Gene expression was calculated by ΔΔCt method.

### Microarray analysis

Microarrays were conducted by the DKFZ Genomics and Proteomics core facility. In brief, total RNA from tumor cells was used to generate libraries which were hybridized on Affymetrix GeneChip™ Mouse Gene 2.0 ST arrays (Affymetrix). Microarray data were normalized using Affymetrix Expression Console software and differential gene expression

Europe PMC Funders Author Manuscripts

was calculated using Affymetrix Transcriptome Analysis Console. Gene Set Enrichment Analysis (GSEA) and Ingenuity Pathway Analysis (IPA) were performed to annotate the differentially regulated molecular pathways. The microarray data with the description are deposited under GEO accession no. GSE146320.

### Seahorse analysis

Mitochondrial function of tumor cells was measured using Mito stress test in XF96 extracellular flux analyzer (Seahorse Bioscience) according to the manufacturer's instruction. Tumor cells (10,000 per well) were seeded in a 96-well Seahorse cell culture plate and incubated overnight. Next day, the cells were shifted to 1% $O_2$ condition (Hypoxia) for 6h at 37°C. After hypoxia treatment, the cells were washed twice and the media was replaced with DMEM sea horse media (Seahorse Bioscience) containing 1mM pyruvate (Sigma), 2mM glutamine (Gibco), and 10mM glucose (Sigma). Next, the plate containing the cells was kept in non-humidified 37°C incubator 1h prior to start of the experiment. Oxygen consumption rate (OCR) was measured at the basal level and after addition of the following compounds: oligomycin (Sigma, 0.5 μM), FCCP, (Sigma, 0.25 μM) and rotenone (Sigma, 0.5 μM). The data were analyzed using the wave software (Seahorse Bioscience) according to the manufacturer's instructions. Proton leak was calculated by subtracting non-mitochondrial respiration from minimum rate measurement after oligomycin injection.

### TCGA analysis

Spearman correlation analysis of TCGA gene expression datasets from Skin Cutaneous Melanoma (SKCM) samples was performed using GEPIA web portal.

### Human Protein Atlas analysis

Kaplan-Meier graphs were plotted from the survival information of melanoma patients extracted from Human Protein Atlas database.

### Transmission electron microscopy

Transmission electron microscopy was performed in the DKFZ electron microscopy core facility. Tumor cells were grown on punched Aklar (EMS, Germany) under serum-starvation and hypoxic conditions for 24h. Thereafter, cells were fixed in buffered aldehyde (4% formaldehyde, 2% glutaraldehyde, 1mM $MgCl_2$, 1mM $CaCl_2$ in 100mM Ca-cacodylate, pH 7.2), post-fixed in aqueous 1% osmium tetroxide followed by en-block staining in 1% ethanolic (75%)-uranylacetate. Following dehydration in graded steps of ethanol, the adherent cells got flat-embedded in epoxide (Glycidether, NMA, DDSA: Serva, Germany). Ultrathin 50nm sections were cut and contrast-stained with lead-citrate and uranylacetate. The sections were imaged with a Zeiss EM910 at 120kV (Carl Zeiss, Germany) and micrographs were taken with a CCD-Camera (TRS, Germany). Mitochondria with disrupted cristae structure were counted and quantification was done manually without prior-knowledge of biological groups.

### Statistical analysis

All data are expressed as mean with error bars depicted as SD or SEM (indicated in figure legends). n represents the number of independent experiments in case of *in vitro* experiments and the number of mice for *in vivo* experiments. Statistical analyses were performed using GraphPad Prism 6. Comparisons between two groups were made using two-tailed unpaired Student's t-test, non-parametric Mann Whitney U-test, or paired t-test. A p-value of less than 0.05 was considered statistically significant.

## Results

### Tumor cells in melanoma patients express ANGPT2

To investigate the abundance and cellular source of ANGPT2 in melanoma patients, we performed immunohistochemical staining of ANGPT2 in primary tumors and metastatic tissue biopsies. In line with previous publications, a substantial fraction (26/68) of melanoma biopsies expressed high levels of ANGPT2 (Fig. 1A, Supplementary Fig. S1A, B). A closer look at the stained tissue micro-arrays (TMA) revealed two different staining patterns – one in which ANGPT2 was confined to blood vessels (Fig. 1A, upper image) and a second with more diffuse pleiotropic presence of ANGPT2 (Fig. 1A, lower image), thereby hinting to different cellular sources of secreted ANGPT2. To conclusively determine the source of ANGPT2 in tumor tissues, we employed *in situ* hybridization (ISH)-based staining of *ANGPT2* mRNA in an independent melanoma TMA. Indeed, ISH analysis demonstrated that tumor cells, in addition to EC, expressed *ANGPT2* in a subset of melanoma biopsies (Fig. 1B). Forty-seven of 133 analyzed samples (using ISH) had detectable *ANGPT2* expression (Supplementary Fig. S1A) and 23 of these showed *ANGPT2* expression in tumor cells. Since serum levels of ANGPT2 had been shown to correlate with prognosis of melanoma patients, we assessed whether tumor cell-expressed *ANGPT2* could serve as a predictive biomarker for melanoma progression (6). Indeed, a higher fraction (28.2%) of metastatic melanoma patient biopsies had *ANGPT2* expression in tumor cells when compared with primary tumor and benign nevi samples (Fig. 1C). This implied that increased ANGPT2 expression in tumor cells was associated with metastatic progression. Moreover, analysis of Human Protein Atlas datasets revealed an inverse correlation between *ANGPT2* expression levels and overall survival of melanoma patients (Supplementary Fig. S1C). Taken together, human melanoma cells express and secrete ANGPT2 and *ANGPT2* expression is a prognostic marker for metastatic melanoma.

### *Angpt2* silencing in tumor cells enhances intratumoral necrosis

To examine the functional role of tumor cell-derived ANGPT2, a set of human and mouse melanoma cell lines was screened for *ANGPT2* gene expression, wherein 5/8 human (Supplementary Fig. S1D) and 2/2 mouse (Fig. 1D) melanoma cell lines were found positive for *ANGPT2* expression. Side-by-side comparison of *ANGPT2* expression levels in tumor cells with the corresponding mouse or human EC showed that mouse tumor cells had endogenous *Angpt2* levels similar to murine lung EC, whereas human melanoma cells expressed *ANGPT2* to a lower extent compared with HUVEC. Despite significant *Angpt2* expression, both murine melanoma cell lines lacked detectable expression of the cognate signaling receptor Tie2 (*Tek*; Fig. 1D). In the case of human tumor cells, 8/8 cell lines

displayed low but detectable levels of *TEK* (Supplementary Fig. S1E). Based on endogenous *ANGPT2* expression, we chose 3 cell lines, including 2 murine (RET, B16F10) and 1 human (SKMEL-28), with relatively higher *ANGPT2* expression to determine whether these cell lines secreted ANGPT2. Indeed, all three tested cell lines secreted ANGPT2 with conditioned media concentrations ranging from 0.44 ng/ml in SKMEL-28 to 2.4 ng/ml and 3.8 ng/ml in B16F10 and RET cell lines, respectively (Fig. 1E, Supplementary Fig. S1F). Tumor cell-secreted ANGPT2 may act either in a paracrine manner on stromal cells (EC, $Tie2^+$ macrophages) or in an autocrine manner on melanoma cells. Considering that both, RET and B16F10 cells secreted much higher amounts of ANGPT2 as compared with SKMEL-28 cells, we selected these two melanoma cells for further experimentation. Additionally, the syngeneic status of RET and B16F10 cells allowed us to perform all *in vivo* experiments in immunocompetent mice, thereby assessing the impact of tumor cell-derived ANGPT2 on all stromal components of the tumor microenvironment.

To study the functional role of tumor cell-derived ANGPT2 during tumor progression, shRNA mediated knockdown of *Angpt2* was performed in RET and B16F10 cells. Effective silencing of *Angpt2*, both at the mRNA and protein levels, was achieved *in vitro* using two independent shRNAs (sh-1 and sh-2; Fig. 1E, Supplementary Fig. S2A). Reduced expression of *Angpt2* did not affect the proliferation of tumor cells in an *in vitro* MTT-based assay (Supplementary Fig. S2B). Next, to examine whether the lack of tumor cell-derived ANGPT2 affected primary tumor growth, $1x10^6$ control (non-targeting) or *Angpt2*-silenced tumor cells (RET and B16F10) were implanted subcutaneously in C57BL/6N mice. Mice were sacrificed 14 days after tumor inoculation and primary tumor weights were measured (Fig. 2A, Supplementary Fig. S3A, B). QPCR analysis of whole tumors verified a significant downregulation of *Angpt2* in both experimental models (Fig. 2B, Supplementary Fig. S3C). Further, ELISA-based quantitation confirmed a significant reduction of ANGPT2 protein in *Angpt2*-depleted primary tumors (Supplementary Fig. S3D). In line with our previous *in vitro* observations, no significant difference was observed in primary tumor growth between the non-targeting control and *Angpt2*-silenced tumors. In-depth histological analysis of tumor tissue sections revealed that *Angpt2*-silenced tumors had higher intratumoral necrosis in both tumor models as compared with control tumors (Fig. 2C, Supplementary Fig. S3E, F). Further, qPCR (Supplementary Fig. S3G, H) and immunofluorescence (IF) (Fig. 2D, Supplementary Fig. S3I, J) analyses of the proliferation maker Ki67 did not show differences between control and *Angpt2*-silenced primary tumors, indicating that enhanced necrosis did not result in a reduction of tumor cell proliferation. Reintroduction of *Angpt2* expression in *Angpt2*-depleted tumor cells abolished the intratumoral necrosis associated with the loss of *Angpt2* in tumor cells (Fig. 2E, F). Thus, enhanced necrosis in *Angpt2*-depleted tumors is resulting specifically from the ack of *Angpt2* and was not due to potential shRNA off-target effects. Overall, the data suggested that tumor cell-derived ANGPT2 was largely dispensable for primary tumor growth and suppressed intratumoral necrosis.

## Tumor cell-derived ANGPT2 does not alter tumor stroma

EC-derived ANGPT2 acts autocrine on blood vessels, thereby priming otherwise, quiescent EC for sprouting angiogenesis (9). We therefore hypothesized that tumor cell-secreted ANGPT2 might act similarly to facilitate tumor neoangiogenesis and potentially defunct

neoangiogenesis might have resulted in the increased intratumoral necrosis as observed in *Angpt2*-silenced tumors. To this end, the tumor vasculature was analyzed in control and *Angpt2*-silenced primary tumor samples. The IF-based vascular analysis revealed that the absence of tumor cell-secreted *Angpt2* affected neither microvessel density nor pericyte coverage in both melanoma models (Supplementary Fig. S4A-D). Thus, the data excluded apparent effects of cancer cell-derived ANGPT2 on the tumor vasculature, possibly suggesting that stromal-derived ANGPT2 was sufficient to sustain tumor neoangiogenesis.

Recently, ANGPT/TIE signaling has been shown to regulate tumor immune surveillance. Mechanistically, dual-inhibition of ANGPT2 and VEGFA resulted in increased tumor necrosis and enhanced antigen presentation by intratumoral phagocytes which eventually led to an increase in infiltration of CD8+ cytotoxic T-cells (15). This prompted us to test whether the increased necrosis in *Angpt2*-silenced tumors might be attributed to alterations in immune cell infiltration. FACS-based immune phenotyping revealed no significant differences in either lymphoid (Fig. 3A, Supplementary Fig. S4E) or myeloid (Fig. 3B, Supplementary Fig. S4F) cell populations when comparing non-targeting control and *Angpt2*-silenced tumors. Therefore, the data ruled out a possible contribution of immune cells in enhancing tumor necrosis in *Angpt2*-silenced tumors.

## ANGPT2 affects intracellular oxidative stress signaling

With no detectable alterations in the vascular architecture and immune cell infiltration, we next investigated possible autocrine effects of *Angpt2* silencing on tumor cells. To this end, global transcriptomic profiling of *in vitro*-cultured non-targeting control and *Angpt2*-silenced tumor cells was performed to trace changes of transcriptional gene signatures. Gene set enrichment analysis (GSEA) revealed that *Angpt2* knockdown in tumor cells perturbed cellular redox homeostasis as indicated by the enrichment of gene sets involved in the biosynthesis of reactive oxygen species (ROS) and subsequent cell death in response to oxidative stress (Fig. 4A). Additionally, pathways regulating metastasis, the antioxidant stress response and mitochondrial function were found regulated in *Angpt2*-silenced tumor cells (Fig. 4A, Supplementary Fig. S5A, B). Indeed, the NFE2L2 (NRF2) signaling pathway, which underlines one of the major cellular defense mechanisms to resolve cellular oxidative stress, was found downregulated in *Angpt2*-silenced tumor cells (Fig. 4A) (16). Therefore, enhanced production of ROS together with crumbling cellular antioxidative defense mechanisms may have led to elevated levels of intracellular oxidative stress in the absence of *Angpt2* expression. Indeed, *in silico* analysis of TCGA human skin cutaneous melanoma (SKCM) dataset revealed a positive correlation between *ANGPT2* and *NFE2L2* expression (Fig. 4B), substantiating our findings from *Angpt2*-deficient murine melanoma cells. Furthermore, the expression of *HMOX1*, a key downstream enzyme in the NRF2 signaling cascade and scavenger for cellular ROS (16), also positively correlated with *ANGPT2* in the TCGA-SKCM dataset (Fig. 4B).

To confirm these *in vitro* findings *in vivo*, we assessed the expression of *Hmox1* in control and *Angpt2*-silenced tumors. Corroborating our earlier findings, *Angpt2*-silenced tumors manifested lower expression of *Hmox1* as compared with control tumors (Fig 4C, Supplementary Fig. S6A). To examine whether the reduced expression of *Hmox1* resulted in

perturbed redox homeostasis, intracellular ROS levels were measured in tumor cells isolated from primary tumors. Increased ROS levels were detected in *Angpt2*-silenced as compared with control tumor cells, thereby implying a malfunctioning redox homeostasis (Fig. 4D, Supplementary Fig. S6B). Interestingly, *in vitro*-cultured *Angpt2*-deficient tumor cells did not show any change in ROS production under normal culture conditions as compared with control cells (Supplementary Fig. S6C). Yet, under serum starvation, *Angpt2* silencing led to a significant increase in intracellular biosynthesis of ROS (Supplementary Fig. S6C), possibly capturing the nutrition-deprived *in vivo* conditions. Further, restoring *Angpt2* expression in *Angpt2*-silenced tumor cells rescued the ROS levels to homeostatic conditions (Supplementary Fig. S6D).

Enhanced ROS production has previously been reported to induce necrosis (5). This led us to hypothesize that increased ROS levels in *Angpt2*-depleted tumors could have resulted in the observed necrosis phenotype. To further experimentally validate this hypothesis *in vivo*, mice implanted with either control or *Angpt2*-silenced tumor cells were administered ROS inhibitor N-acetyl-L-cysteine (NAC) in drinking water (Supplementary Fig. S6E). NAC treatment abrogated the previously-observed increase in intratumoral necrosis in *Angpt2*-depleted as compared with non-targeting control tumors (Fig. 2C, Supplementary Fig. S6F, G). These data indicated that enhanced intracellular ROS in *Angpt2*-depleted tumors may have resulted in increased intratumoral necrosis.

The rapid growth of a primary tumor is often accompanied by nutrient deprivation and induction of hypoxia in the center of tumor tissue (17). Such a hostile environment can have detrimental effects on mitochondrial function in tumor cells. Subsequently, mitochondria lose their morphology and cristae structure, essential determinants of their physiological function, and begin to produce high levels of ROS (18,19). To investigate whether mitochondrial morphology was altered in *Angpt2*-silenced tumor cells, we performed ultrastructural analyses of tumor cells cultured under different conditions (hypoxia and serum starvation) by transmission electron microscopy. Under normoxic conditions, no significant differences in the mitochondrial structure was observed upon *Angpt2* knockdown (Supplementary Fig. S7A, B). Yet, under hypoxic conditions, mitochondrial morphology was highly irregular with near-complete loss of cristae structure in *Angpt2*-silenced as compared with control tumor cells (Fig. 4E). Concurrently, the number of fragmented mitochondria per cell was significantly increased (Fig. 4F). Expression analysis of genes involved in mitochondrial dynamics showed a reduced expression of Drp1 (*Dnm1l*) and *Fis1* in *Angpt2*-depleted primary tumors (Supplementary Fig. S7C, D). DRP1 and FIS1 are required for maintaining mitochondrial integrity, therefore their downregulation highlights perturbation in mitochondrial function in the absence of *Angpt2* expression (20,21).

To determine an unambiguous readout of mitochondrial function, a Seahorse Mito Stress experiment was conducted to determine the mitochondrial bioenergetic profile of tumor cells. Proton leak, a key parameter in a Seahorse experiment, represents the oxygen consumption rate (OCR) associated with all ion movement across the inner mitochondrial membrane during ATP synthesis (22). Indeed, the loss of ANGPT2 resulted in a significant reduction of proton leak in tumor cells, thereby confirming diminished mitochondrial function (Fig. 4G). Furthermore, elevated ROS levels, due to curtailed mitochondrial

function, have been shown to activate MAPK stress signaling (23). Concomitantly, increased phosphorylation levels of ERK and P38, key components of the MAPK pathway, were observed in *Angpt2*-silenced primary tumors when compared with control tumors (Fig. 4H, Supplementary Fig. S7E). Overall, the data established an important role of tumor cell-expressed *Angpt2* in maintaining mitochondrial function and redox homeostasis.

### Tumor cell-expressed *Angpt2* facilitates metastasis

To investigate if *Angpt2* deficiency affected the metastatic potential of melanoma cells, tumor cells were intravenously injected to initiate an experimental metastasis assay. Loss of tumor cell-expressed *Angpt2* resulted in a significant reduction in lung metastases in both melanoma models (Fig. 5A, B, Supplementary Fig. S8A, B). To circumvent the substantial heterogeneity of the experimental metastasis assay, we performed an indexed analysis by co-injecting RFP-labeled control and GFP-labeled *Angpt2*-silenced cells in mice and measured the composition of lung metastases *ex vivo* 14 days after intravenous injection. Unambiguously, *Angpt2*-silenced tumor cells exhibited reduced metastatic potential as compared with control cells (Fig. 5C, D, Supplementary Fig. S8C, D). Moreover, rescuing *Angpt2* expression in Angpt2-depleted cells reversed the observed decline in metastasis (Fig. 5E, F), thereby indicating that reduction of metastasis was due to the loss of *Angpt2*. Next, we employed a cervical LN metastasis model in which intradermally-inject tumor cells in the ear colonize the draining LN. Similar to the lung experimental metastasis assay, depletion of tumor cell-*Angpt2* reduced the incidence of cervical LN metastasis (Fig. 5G, H). To substantiate the findings in a spontaneous metastasis model, we utilized the LLC post-surgical model in which lung metastases develop after surgical removal of the primary tumor (Supplementary Fig. S8E). Indeed, there was a significant decrease in post-surgical survival of mice implanted with *Angpt2*-overexpressing as compared with control LLC cells (Supplementary Fig. S8F, G).

Based on the above findings, we hypothesized that the observed decrease in metastatic capability of *Angpt2*-depleted cells could be due to enhanced oxidative stress. To experimentally investigate this hypothesis, mice injected intravenously with either control or *Angpt2*-silenced RET cells were treated with ROS scavenger NAC. In line with the primary tumor data, administration of NAC in mice injected with *Angpt2*-deleted tumor cells rescued the observed reduction of metastasis upon loss of *Angpt2* in tumor cells (Fig. 6A-C). Collectively, these experiments underline tumor cell-expressed *Angpt2* as a crucial regulator of their metastatic capability, primarily by altering intracellular ROS and subsequent cellular oxidative stress.

Next, we performed a set of experiments to mechanistically decipher the role of tumor cell-expressed *Angpt2* on different steps of the metastatic cascade experienced by the tumor cells in an experimental metastasis model. Examining the role of migration, anoikis-induced tumor cell death, tumor cell adhesion to EC and to ECM depicted no significant differences between control and *Angpt2*-silenced tumor cells, suggesting that tumor cell-expressed *Angpt2* did not impact early steps of the metastatic cascade (Supplementary Fig. S9A-H). Subsequently, we assessed whether tumor cell-derived ANGPT2 was required for tumor cell invasion and transmigration. Downregulation of *Angpt2* hindered the capability of tumor

cells to invade through the basement membrane and transmigrate across the endothelial barrier (Supplementary Fig. S10A-H). Further, we evaluated whether tumor cell-expressed *Angpt2* affected the ability of tumor cells to colonize the metastatic site. To simulate *in vivo* conditions for colonization, tumor cells were treated under anoikis conditions for 48h and a colony formation assay was initiated thereafter. Lack of *Angpt2* decreased the colonization potential of tumor cells as indicated by sharp reduction in the number of colonies (Supplementary Fig. S11A-D). Concordantly, overexpressing *Angpt2* in *Angpt2*-depleted tumor cells recovered the colonizing capability of the tumor cells (Supplementary Fig. S11E,F). These findings demonstrate that tumor cell-expressed *Angpt2* promoted metastasis by facilitating the colonization process.

## Discussion

The incidence of melanoma has been steadily rising during the last 50 years. While the 5-year survival rate for patients with locally-contained (stage I) melanoma is 98%, distant metastasis is often life-threatening with a modest survival rate of 23% (1). This can largely be attributed to early metastatic spread and non-reliable detection of primary lesions. It is estimated that approximately 10% of melanomas go undetected with the current diagnostic methods (4). Previously, we have established serum ANGPT2 as a reliable biomarker for melanoma progression, especially to distinguish stage III/IV from primary melanomas (8). Indeed, patients with distant organ metastasis (stage IV) had on average 4-fold higher levels of serum ANGPT2 when compared with patients with lymph-node (LN)-restricted tumors (stage III). Intriguingly, immunoperoxidase-based analysis of advanced-stage tumors revealed a weak but consistent expression of ANGPT2 in tumor cells. These data raised the question of relative abundance and functional role of tumor cell-expressed ANGPT2 during melanoma metastasis.

Employing a wide array of clinical and preclinical analysis, the present study demonstrates that (1) tumor cells serve as a source of ANGPT2 in a fraction of melanoma patients; (2) loss of endogenous *Angpt2* expression in tumor cells neither affects primary tumor growth, nor does it influence tumor angiogenesis and the immune landscape, but rather results in enhanced intratumoral necrosis; (3) *Angpt2* silencing in tumor cells perturbed cellular redox homeostasis by augmenting mitochondrial dysfunction; and (4) *Angpt2* silencing in melanoma cells profoundly suppressed lung metastases due to enhanced ROS production, which led to reduction in colonization potential of *Angpt2*-silenced tumor cells. Together, these data reveal novel functions of cancer cell-derived ANGPT2 during melanoma progression.

Following the clinical approval of VEGF/VEGFR-targeting drugs, ANGPT/TIE signaling was pursued as second generation angiogenesis-regulating vascular tyrosine kinase system for its ability to synergistically enhance the efficacy of approved anti-angiogenic therapies (5). Similar to VEGF, ANGPT2 was found upregulated in both primary tumor tissues and the circulation of multiple cancer entities. Yet, whereas VEGF is primarily secreted by the tumor cells, ANGPT2 is almost exclusively produced by tumor-associated EC (24). Yet, some melanoma biopsies from patients with advanced disease manifested a rather diffuse staining of ANGPT2 compared with the confined blood vessel-restricted staining in other

tumors. Likewise, several cultured human melanoma cell lines have been reported to express ANGPT2 (8). Here, employing *in situ* hybridization, we unambiguously traced the cellular source of ANGPT2 in human tissue microarrays. Clearly, tumor cells in a subset of human melanomas expressed and secreted ANGPT2. However, unlike the granular pattern of ANGPT2 staining observed in EC due to its localization in Weibel-Palade bodies, ANGPT2 staining in TMA sections had a uniform cytoplasmic localization pattern in tumor cells (25). This suggests that ANGPT2 in tumor cells may not be stored and rapidly released upon stimulation.

Evaluation of ANGPT2 expression in melanoma patient samples demonstrated that the fraction of patients with tumor cell-expressed ANGPT2 was much higher in the metastatic specimens as compared with either nevus or primary melanomas, thereby suggesting a crucial role of tumor cell-expressed ANGPT2 for melanoma metastasis.

Host-derived ANGPT2 has been shown to affect early stages of primary tumor growth but is largely dispensable for the growth of established tumors (6). Concurrently, administration of ANGPT2-neutralizing antibody delayed primary tumor growth of xenografted human cells (26). Mechanistically, ANGPT2-blockade restricted EC proliferation and enhanced pericyte coverage for improved perfusion properties. Apart from the proangiogenic function of ANGPT2, ectopic overexpression of ANGPT2 in human breast cancer cells has been described to act autocrine, thereby promoting cellular invasiveness to facilitate distant metastasis (27). Likewise, ANGPT2 overexpression in glioma cells induced tumor cell invasion in an MMP2-dependent manner (28). Thus, previous publications have hinted towards an autocrine, angiogenesis-independent role of cancer cell-expressed ANGPT2 during tumor progression. However, the previous studies have relied on exogenous overexpression of ANGPT2, which often tends to flood the cellular environment with non-physiological amounts of protein, thereby interfering with their normal cellular function (29). To circumvent this artificial gain-of-function approach, we utilized two mouse melanoma cell lines, RET and B16F10, with high endogenous expression of *Angpt2*, similar to mouse lung EC. ShRNA-mediated knockdown of *Angpt2* in tumor cells did not alter primary tumor growth. Further, tumor cell-specific silencing of *Angpt2* neither affected tumor vasculature nor the immune milieu. The loss of tumor cell-secreted ANGPT2 was possibly compensated by the host endothelium. Surprisingly though, primary tumors arising from *Angpt2*-silenced melanoma cells displayed increased intratumoral necrosis when compared with non-targeting control tumors, thereby emphasizing a protective role of tumor cell-expressed *Angpt2* during primary tumor growth.

Comparative transcriptomic analysis of control and *Angpt2*-silenced tumor cells identified perturbations in intracellular redox homeostasis. *Angpt2* deficiency in tumor cells positively correlated with gene sets involved in ROS biosynthesis and subsequent cell death due to oxidative stress. In turn, lack of ANGPT2 led to downregulation of NFE2L2 targets. NFE2L2 (Nrf2), an upstream transcriptional regulator for multiple ROS-scavenging enzymes, protects a cell from oxidative damage (16). Indeed, tumors arising from *Angpt2*-silenced melanoma cells showed reduced expression of *Hmox1* (a downstream effector of NFE2L2), and recorded higher levels of intracellular ROS as compared with control tumors. Moreover, antioxidant treatment of mice bearing *Angpt2*-depleted primary tumors resulted

in reduction of overall intratumoral necrosis. This implied that intracellular ROS generated after *Angpt2*-silencing in tumor cells drives necrosis in primary tumors. Correspondingly, analysis of TCGA-SKCM data set revealed a positive correlation between *ANGPT2* and *NFE2L2/HMOX1* expression, further bolstering a crucial role of tumor cell-expressed *ANGPT2* in minimizing stress-induced oxidative damage.

Unrestricted growth of primary tumors results in a hypoxic and nutrient-deprived core (30). In a hypoxic microenvironment, tumor cells adapt their mitochondrial function to slow down oxidative phosphorylation and hyperactivate NRF2 pathway to lower intracellular levels of ROS (19). Any imbalance in these protective mechanisms may result in the accumulation of ROS and sustained oxidative damage. Melanoma cells quickly adapt to the hypoxic conditions as they did not display major alterations in the mitochondrial ultrastructure. Nevertheless, in the absence of *Angpt2* expression, melanoma cells witnessed a higher fraction of dysfunctional mitochondria and subsequent reduction in energy production. Hence, enhanced expression of *Angpt2* in melanoma tumor cells acts as a defense mechanism against cellular stress. These findings are in line with a recent publication highlighting the protective role of ANGPT2 on hepatocellular cancer cell line HepG2 under Doxorubin-induced cytotoxic stress by reducing ROS production and preserving mitochondrial function (31).

Despite no apparent effects on primary tumor growth, *Angpt2*-silenced melanoma cells led to reduced lung metastasis in experimental metastasis assays. Mechanistically, *Angpt2* silencing restricted the efficacy of metastatic colony formation of melanoma cells. Likewise, ectopic expression of ANGPT2 in PDAC xenografts was reported to display an enhanced rate of lymphatic metastasis (32). Successful colonization at a distant organ site requires a single-seeded tumor cell to survive in a hostile microenvironment and to overcome a variety of extracellular and intracellular stresses. Our molecular data underline an important role of tumor cell-expressed *Angpt2* in maintaining intracellular oxidative balance and preserving mitochondrial function. Notably, ROS scavenger NAC effectively reinstated the metastatic capacity of *Angpt2*-depleted tumor cells. Thus, tumor cell-*Angpt2* protects melanoma cells from oxidative stress and ensures their survival during the metastasis process. These mechanistic findings explain why a higher fraction of metastatic melanoma biopsies displayed tumor cell-expressed ANGPT2.

In summary, the present study, by establishing spatial distribution of ANGPT2 expression in metastatic melanoma, has revealed the cellular source of ANGPT2 in melanoma and shed light on the molecular and functional contribution of tumor cell-expressed *Angpt2* during metastasis. The findings expand the hitherto endotheliocentric view of angiopoietin functions and validate ANGPT2 as a therapeutic target for a well-defined subset of melanoma patients.

## Supplementary Material

Refer to Web version on PubMed Central for supplementary material.

## Acknowledgements

We would like to thank Dr. Karsten Richter and Dr. Michelle Neßling from the DKFZ electron microscopy core facility for their assistance in acquiring electron microscopy images. We would like to thank Dr. Suzana Vega Harring from Roche for performing the ANGPT2 staining. We would like to thank Dr. Damir Krunic from the DKFZ light microscopy facility for his assistance in image analysis. The DKFZ flow cytometry, light microscopy, genomics and proteomics, and laboratory animal core facilities are gratefully acknowledged for their excellent support. This work was supported by grants from the Deutsche Forschungsgemeinschaft [project FE 1282/2-1 to M. Felcht]; DFG-funded Research Training Group 2099 “Hallmarks of Skin Cancer” [project number 259332240 to H.G. Augustin, M. Felcht, C. Géraud, S. Goerdt and J. Utikal]; the DFG-funded Collaborative Research Center CRC-TR209 “Hepatocellular Carcinoma” [project C3 to S. Goerdt and H. G. Augustin], and the European Research Council Advanced Grant “AngioMature” [project 787181 to H. G. Augustin].

## References

1. Siegel RL, Miller KD, Jemal A. Cancer statistics, 2019. CA Cancer J Clin. 2019; 69:7–34. [PubMed: 30620402]
2. Schadendorf D, Fisher DE, Garbe C, Gershenwald JE, Grob JJ, Halpern A, et al. Melanoma. Nat Rev Dis Primers. 2015; 1 15003 [PubMed: 27188223]
3. Gide TN, Wilmott JS, Scolyer RA, Long GV. Primary and acquired resistance to immune checkpoint inhibitors in metastatic melanoma. Clin Cancer Res. 2018; 24:1260–70. [PubMed: 29127120]
4. Schadendorf D, van Akkooi ACJ, Berking C, Griewank KG, Gutzmer R, Hauschild A, et al. Melanoma. Lancet. 2018; 392:971–84. [PubMed: 30238891]
5. Saharinen P, Eklund L, Alitalo K. Therapeutic targeting of the angiopoietin-TIE pathway. Nat Rev Drug Discov. 2017; 16:635–61. [PubMed: 28529319]
6. Nasarre P, Thomas M, Kruse K, Helfrich I, Wolter V, Deppermann C, et al. Host-derived angiopoietin-2 affects early stages of tumor development and vessel maturation but is dispensable for later stages of tumor growth. Cancer Res. 2009; 69:1324–33. [PubMed: 19208839]
7. Srivastava K, Hu J, Korn C, Savant S, Teichert M, Kapel SS, et al. Postsurgical adjuvant tumor therapy by combining anti-angiopoietin-2 and metronomic chemotherapy limits metastatic growth. Cancer Cell. 2014; 26:880–95. [PubMed: 25490450]
8. Helfrich I, Edler L, Sucker A, Thomas M, Christian S, Schadendorf D, et al. Angiopoietin-2 levels are associated with disease progression in metastatic malignant melanoma. Clin Cancer Res. 2009; 15:1384–92. [PubMed: 19228739]
9. Augustin HG, Koh GY, Thurston G, Alitalo K. Control of vascular morphogenesis and homeostasis through the angiopoietin-Tie system. Nat Rev Mol Cell Biol. 2009; 10:165–77. [PubMed: 19234476]
10. Sfiligoi C, de Luca A, Cascone I, Sorbello V, Fuso L, Ponzone R, et al. Angiopoietin-2 expression in breast cancer correlates with lymph node invasion and short survival. Int J Cancer. 2003; 103:466–74. [PubMed: 12478661]
11. Gu J, Yamamoto H, Ogawa M, Ngan CY, Danno K, Hemmi H, et al. Hypoxia-induced up-regulation of angiopoietin-2 in colorectal cancer. Oncol Rep. 2006; 15:779–83. [PubMed: 16525658]
12. Maffei R, Martinelli S, Castelli I, Santachiara R, Zucchini P, Fontana M, et al. Increased angiogenesis induced by chronic lymphocytic leukemia B cells is mediated by leukemia-derived Ang2 and VEGF. Leuk Res. 2010; 34:312–21. [PubMed: 19616847]
13. Iwamoto T, Takahashi M, Ito M, Hamatani K, Ohbayashi M, Wajjwalku W, et al. Aberrant melanogenesis and melanocytic tumour development in transgenic mice that carry a metallothionein/ret fusion gene. EMBO J. 1991; 10:3167–75. [PubMed: 1915289]
14. Teichert M, Stumpf C, Booken N, Wobser M, Nashan D, Hallermann C, et al. Aggressive primary cutaneous B-cell lymphomas show increased Angiopoietin-2-induced angiogenesis. Exp Dermatol. 2015; 24:424–9. [PubMed: 25776770]

15. Schmittnaegel M, Rigamonti N, Kadioglu E, Cassara A, Wyser Rmili C, Kiialainen A, et al. Dual angiopoietin-2 and VEGFA inhibition elicits antitumor immunity that is enhanced by PD-1 checkpoint blockade. Sci Transl Med. 2017; 9
16. Loboda A, Damulewicz M, Pyza E, Jozkowicz A, Dulak J. Role of Nrf2/HO-1 system in development, oxidative stress response and diseases: an evolutionarily conserved mechanism. Cell Mol Life Sci. 2016; 73:3221–47. [PubMed: 27100828]
17. Petrova V, Annicchiarico-Petruzzelli M, Melino G, Amelio I. The hypoxic tumour microenvironment. Oncogenesis. 2018; 7:10. [PubMed: 29362402]
18. Cogliati S, Enriquez JA, Scorrano L. Mitochondrial cristae: Where beauty meets functionality. Trends Biochem Sci. 2016; 41:261–73. [PubMed: 26857402]
19. Fuhrmann DC, Brune B. Mitochondrial composition and function under the control of hypoxia. Redox Biol. 2017; 12:208–15. [PubMed: 28259101]
20. Fu W, Liu Y, Yin H. Mitochondrial dynamics: Biogenesis, fission, fusion, and mitophagy in the regulation of stem cell behaviors. Stem Cells Int. 2019; 2019 9757201 [PubMed: 31089338]
21. Favaro G, Romanello V, Varanita T, Andrea Desbats M, Morbidoni V, Tezze C, et al. DRP1-mediated mitochondrial shape controls calcium homeostasis and muscle mass. Nat Commun. 2019; 10:2576. [PubMed: 31189900]
22. Divakaruni AS, Brand MD. The regulation and physiology of mitochondrial proton leak. Physiology (Bethesda). 2011; 26:192–205. [PubMed: 21670165]
23. Zhang J, Wang X, Vikash V, Ye Q, Wu D, Liu Y, et al. ROS and ROS-mediated cellular signaling. Oxid Med Cell Longev. 2016; 2016 4350965 [PubMed: 26998193]
24. Rigamonti N, Kadioglu E, Keklikoglou I, Wyser Rmili C, Leow CC, De Palma M. Role of angiopoietin-2 in adaptive tumor resistance to VEGF signaling blockade. Cell Rep. 2014; 8:696–706. [PubMed: 25088418]
25. Fiedler U, Scharpfenecker M, Koidl S, Hegen A, Grunow V, Schmidt JM, et al. The Tie-2 ligand angiopoietin-2 is stored in and rapidly released upon stimulation from endothelial cell Weibel-Palade bodies. Blood. 2004; 103:4150–6. [PubMed: 14976056]
26. Oliner J, Min H, Leal J, Yu D, Rao S, You E, et al. Suppression of angiogenesis and tumor growth by selective inhibition of angiopoietin-2. Cancer Cell. 2004; 6:507–16. [PubMed: 15542434]
27. Imanishi Y, Hu B, Jarzynka MJ, Guo P, Elishaev E, Bar-Joseph I, et al. Angiopoietin-2 stimulates breast cancer metastasis through the alpha(5)beta(1) integrin-mediated pathway. Cancer Res. 2007; 67:4254–63. [PubMed: 17483337]
28. Hu B, Guo P, Fang Q, Tao HQ, Wang D, Nagane M, et al. Angiopoietin-2 induces human glioma invasion through the activation of matrix metalloprotease-2. Proc Natl Acad Sci U S A. 2003; 100:8904–9. [PubMed: 12861074]
29. Moriya H. Quantitative nature of overexpression experiments. Mol Biol Cell. 2015; 26:3932–9. [PubMed: 26543202]
30. De Palma M, Biziato D, Petrova TV. Microenvironmental regulation of tumour angiogenesis. Nat Rev Cancer. 2017; 17:457–74. [PubMed: 28706266]
31. Li T, Liu Z, Jiang K, Ruan Q. Angiopoietin2 enhances doxorubin resistance in HepG2 cells by upregulating survivin and Ref-1 via MSK1 activation. Cancer Lett. 2013; 337:276–84. [PubMed: 23643942]
32. Schulz P, Fischer C, Detjen KM, Rieke S, Hilfenhaus G, von Marschall Z, et al. Angiopoietin-2 drives lymphatic metastasis of pancreatic cancer. FASEB J. 2011; 25:3325–35. [PubMed: 21685330]

Europe PMC Funders Author Manuscripts

## Significance

This study reveals that tumor cells can be a source of ANGPT2 in the tumor microenvironment and that tumor cell-derived ANGPT2 augments metastatic colonization by protecting tumor cells from oxidative stress.

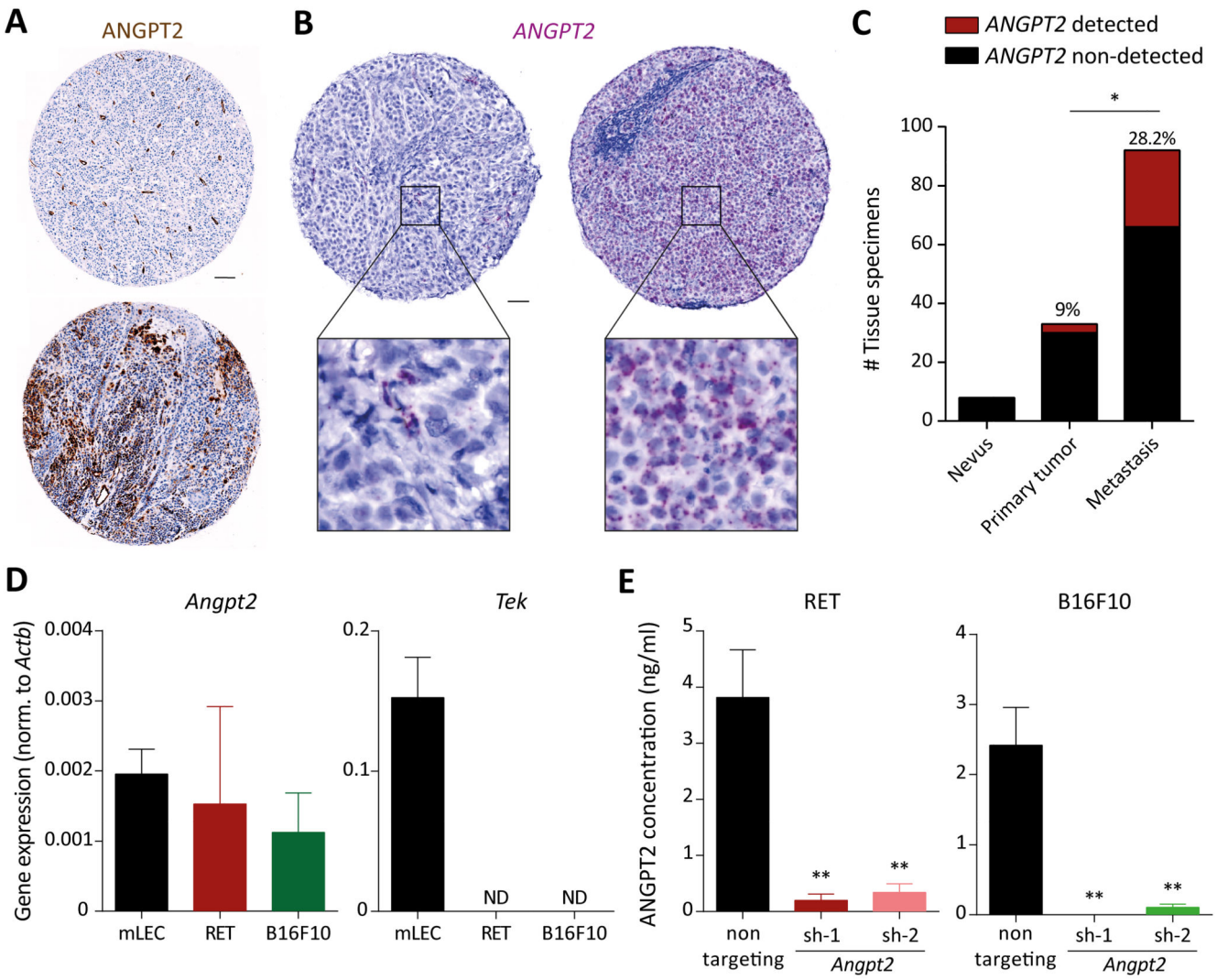


**Figure 1. Melanoma cells express ANGPT2.**

**(A)** Immunohistochemical analysis of ANGPT2 expression in tissue biopsies of human melanomas. Scale bar: 100μM. **(B)** Tissue sections from melanoma patients were stained with *ANGPT2* RNASCOPE probe. Square boxes depict regions of interest (ROIs) at a higher magnification. Scale bar: 50μM. **(C)** Quantitation of the number of patients with detectable expression of ANGPT2 in tumor cells of benign melanocytic nevi (n=8), primary (n=33), and metastatic melanomas (n=92). *, $p<0.05$, Chi-square test. **(D)** *Angpt2* and *Tek* expression were quantified using qRT-PCR in mouse melanoma cell lines and mouse lung EC (ND= non-detected). **(E)** ANGPT2 ELISA was performed to quantify ANGPT2 protein in supernatants of control and *Angpt2* knockdown cells (sh-1 and sh-2) in RET and B16F10n=3; mean ± SD). *, $p<0.05$, **, $p<0.01$, two-tailed unpaired Student's t-test.

Europe PMC Funders Author Manuscripts

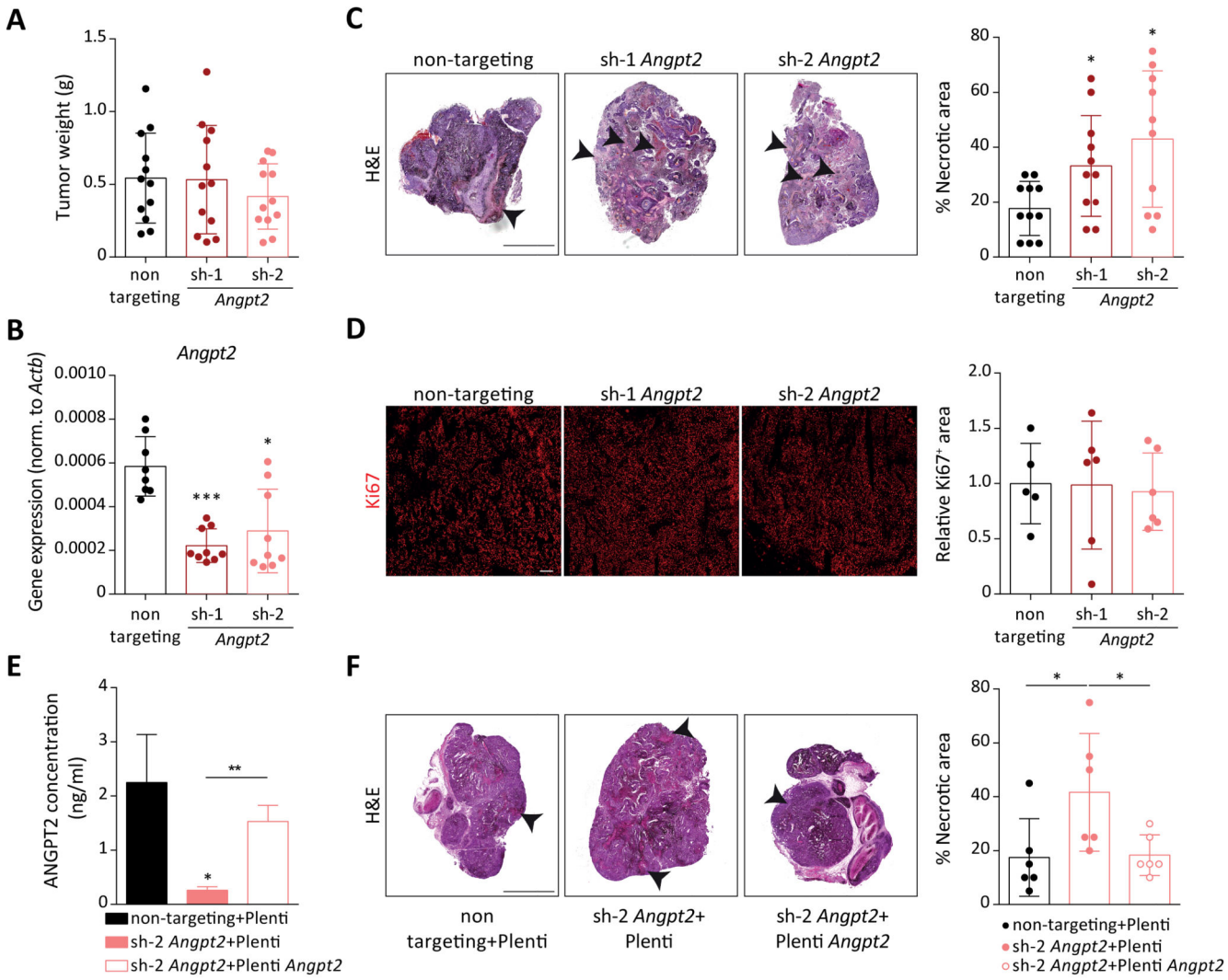


**Figure 2. *Angpt2* knockdown in tumor cells does not alter primary tumor growth.**

**(A)** Tumor weight at day 14 after primary tumor inoculation of control RET and knockdown cell lines (n=12; mean ± SD). **(B)** *Angpt2* expression in control and *Angpt2* knockdown RET primary tumors quantified by qRT-PCR (n=8-9; mean ± SD). *, p<0.05, ****, p<0.0001, Mann Whitney U test. **(C)** On the left, representative H&E images of control and *Angpt2* knockdown RET primary tumors are shown. Arrowheads indicate necrotic area. Scale bar: 1mm. On the right, quantitation of necrotic area is shown (n=9-11 mean ± SD). *, p<0.05, Mann Whitney U test. **(D)** On the left, representative images of tumor sections stained with KI67 (in red). Scale bar: 200μm. On the right, quantitation of KI67-positive area normalized to DAPI area in control and Angpt2 knockdown RET primary tumors (n=5-6; mean ± SD). **(E)** ANGPT2 ELISA was performed to quantify ANGPT2 protein levels in supernatants of control+Plenti, sh-2+Plenti and sh-2+Plenti *Angpt2* cells in RET (n=3; mean ± SD). *, p<0.05, **, p<0.01, two-tailed unpaired Student's t-test. **(F)** On the left, representative H&E images of control+Plenti, sh-2+Plenti and sh-2+Plenti *Angpt2* RET

primary tumors are shown. Arrowheads indicate necrotic area. Scale bar: 1mm. On the right, quantitation of necrotic area is shown (n=6 mean ± SD). *, $p<0.05$, Mann Whitney U test.



Europe PMC Funders Author Manuscripts

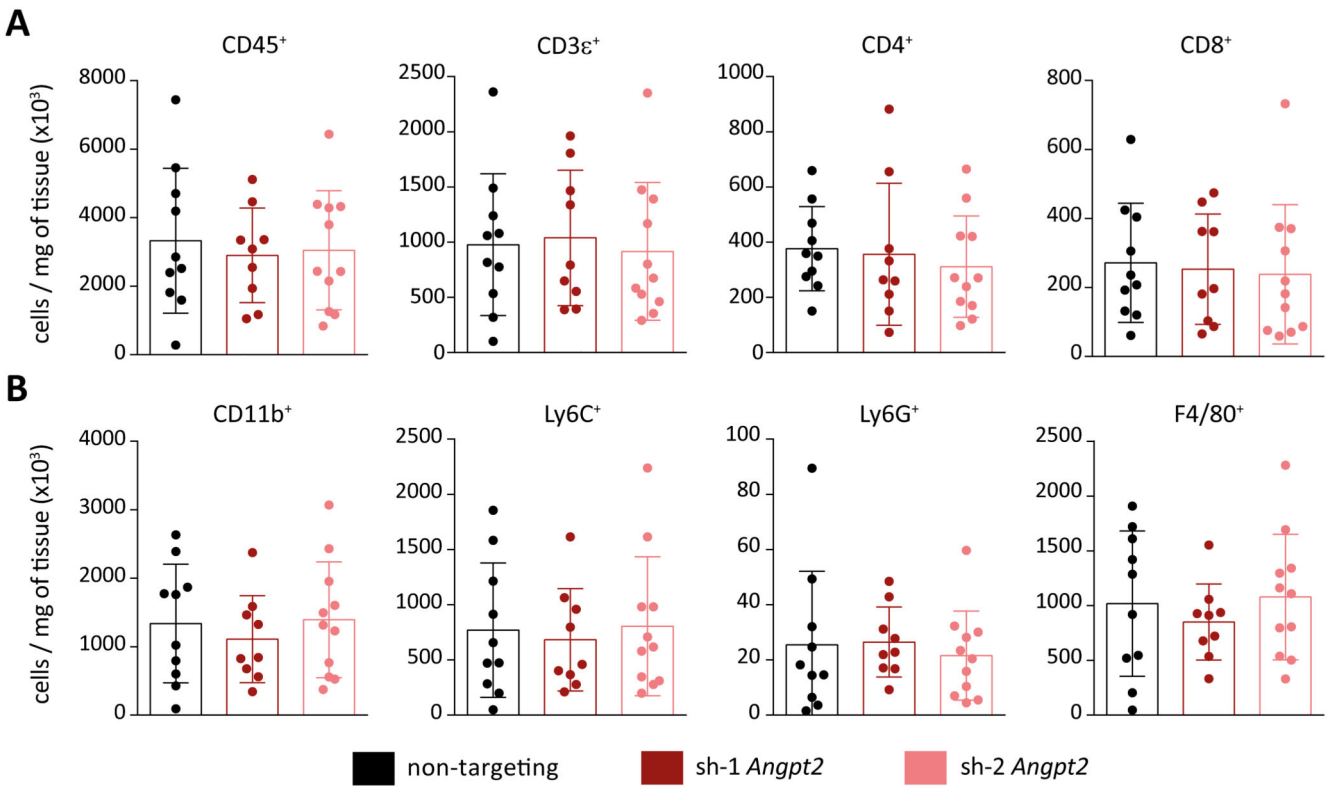


**Figure 3. *Angpt2* knockdown in tumor cells does not impact immune cell infiltration.**

**(A-B)** FACS-based immune analysis was performed control and *Angpt2* knockdown RET primary tumors on day 14 after tumor implantation. Shown are the quantitation of tumor infiltrating lymphoid **(A)** and myeloid cells **(B)** (n=9-11; mean ± SD). All comparisons were rendered non-significant by Mann Whitney U test.




Europe PMC Funders Author Manuscripts

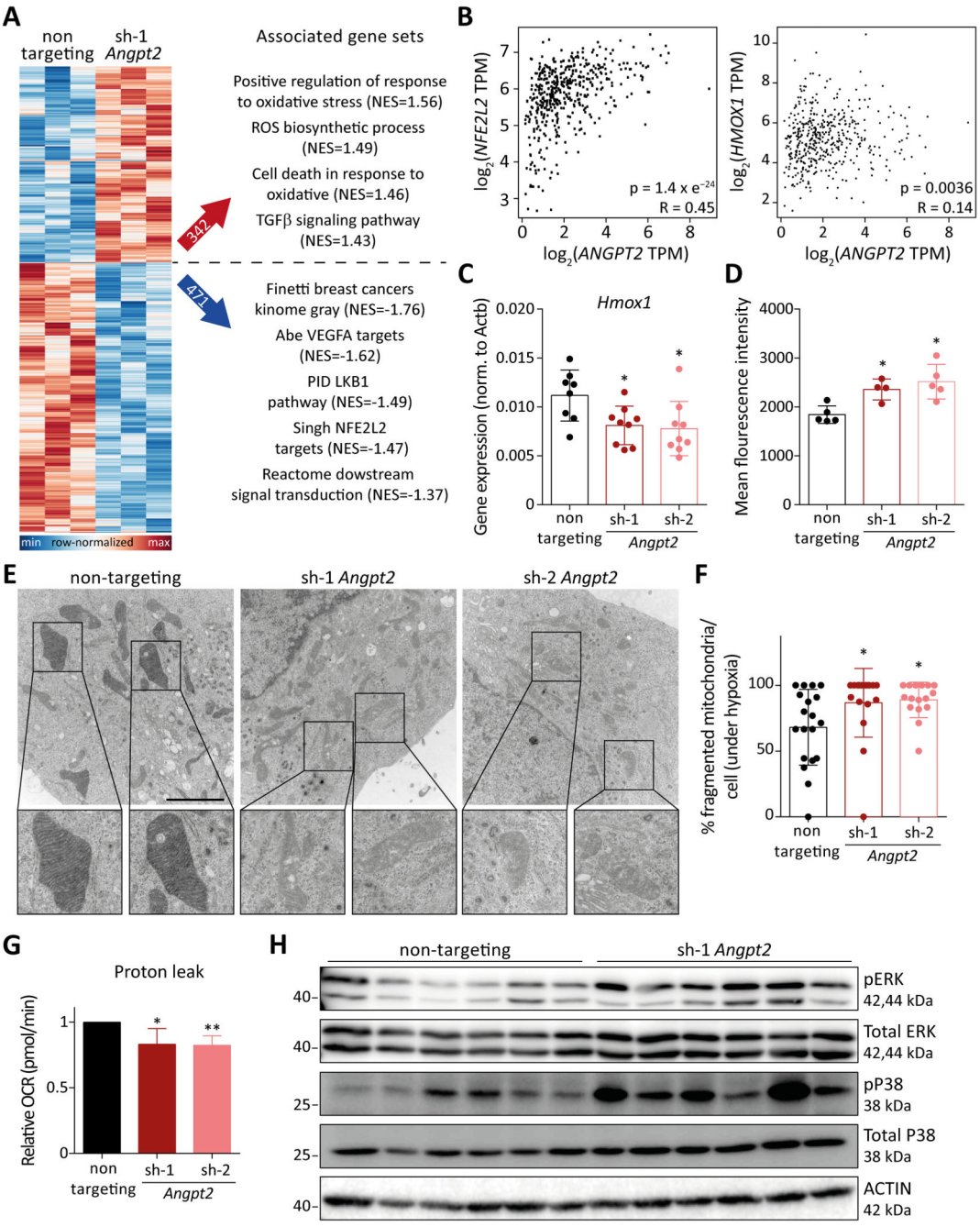


**Figure 4. Tumor cell-expressed *Angpt2* modulates ROS and mitochondrial homeostasis.**

**(A)** On the left, heatmap depicting differentially regulated genes between control- and *Angpt2*-silenced tumor cells. On the right, gene set enrichment analysis identifying alterations in pathways involved in maintaining oxidative homeostasis (NES=normalized enrichment score). **(B)** Spearman correlation analysis of *ANGPT2*, *NFE2L2,* and *HMOX1* in cutaneous melanoma (SKCM) dataset from TCGA database. **(C)** *Hmox1* expression in control and *Angpt2* knockdown RET primary tumors was quantified using qRT-PCR (n=8-9; mean ± SD). *, p<0.05, Mann Whitney U test. **(D)** FACS analysis of ROS levels in control




Europe PMC Funders Author Manuscripts

and *Angpt2* knockdown RET primary tumors (n=4-5; mean ± SD). *, p<0.05, Mann Whitney U test**. (E)** Representative electron microscopic images depicting morphological changes in mitochondria of wild type and *Angpt2*-silenced RET tumor cells. Cells were kept under 1% $O_2$ and serum starvation condition for 24h before processing for electron microscopy. Square boxes depict ROIs at higher magnification. Scale bar: 2μm**. (F)** Quantitation of fragmented mitochondria per cell (n=16-19 cells/condition; mean ± SD). *, p<0.05, Mann Whitney U test. **(G)** Proton leak in control and *Angpt2* knockdown RET tumor cells was measured in a Seahorse Mito Stress experiment. Prior to Seahorse analysis, cells were kept under 1% $O_2$ for 6h (n=5; mean ± SD). *p<0.05, **p<0.01, two-tailed paired Student's t-test. **(H)** Western blot analysis was performed for phospho-ERK, phospho-P38, total-P38, and total-ERK in control and *Angpt2* knockdown RET primary tumors. Actin was used as a loading control (n=6).



Europe PMC Funders Author Manuscripts

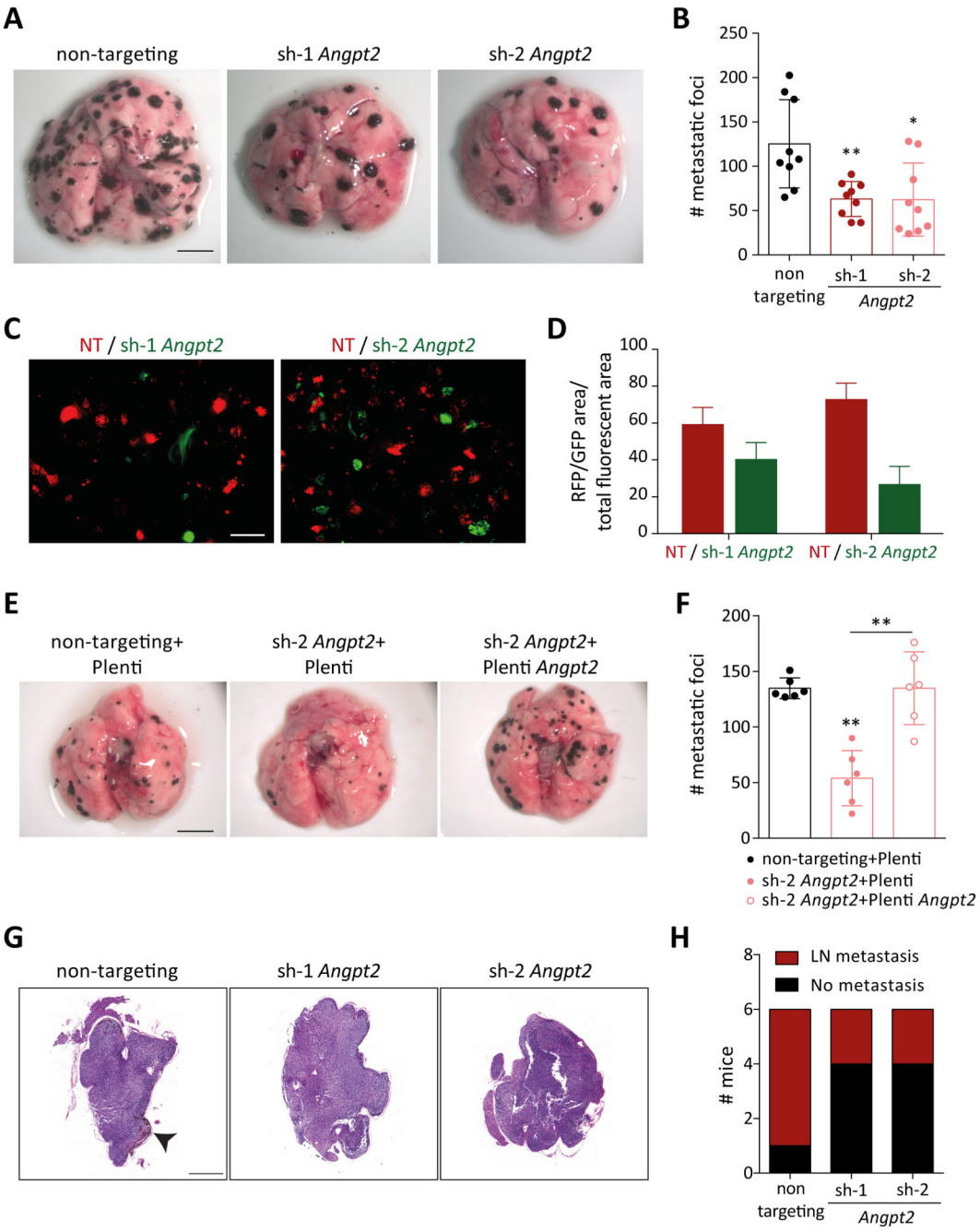


**Figure 5. Tumor cell-expressed *Angpt2* promotes metastasis.**

**(A)** Control or *Angpt2*-deficient RET cells were injected into the tail vein of C57BL/6N mice. Mice were sacrificed after 14 days. Shown are the representative images of lung metastatic foci imaged under a stereomicroscope. Scale bar: 5mm. **(B)** The graph represents the quantitation of lung metastatic foci (n=9; mean ± SD). *, $p<0.05$, **, $p<0.01$, Mann Whitney U test. **(C)** Control (in red) and *Angpt2*-silenced (in green) RET tumor cells were co-injected intravenously in mice. Lungs were harvested 14 days after tumor cell inoculation and visualized under a fluorescent dissection microscope. Representative images of lung

metastatic foci are shown. Scale bar: 2mm. **(D)** Quantitation of lung colonization by control (in red) or *Angpt2*-silenced (in green) RET tumor cells. The area of each metastatic colony (RFP/GFP) was normalized to the combined fluorescent area (n=5-6; mean ± SD). **(E)** Control+Plenti, sh-2+Plenti and sh-2+Plenti *Angpt2* cells were injected into the tail vein of C57BL/6N mice. Mice were sacrificed after 14 days. Shown are representative images of lung metastatic foci imaged under a stereomicroscope. Scale bar: 5mm. **(F)** The graph represents the quantitation of lung metastatic foci (n=6; mean ± SD). **, $p<0.01$, Mann Whitney U test. **(G)** WT C57BL/6N mice were intradermally injected with either 300,000 control or *Angpt2* knockdown RET tumor cells in the ear and regional LN were collected 2 weeks later. Representative H&E images of LN. Arrowheads indicate detectable metastases. **(H)** The incidence of LN metastasis is depicted (n=6).

Europe PMC Funders Author Manuscripts

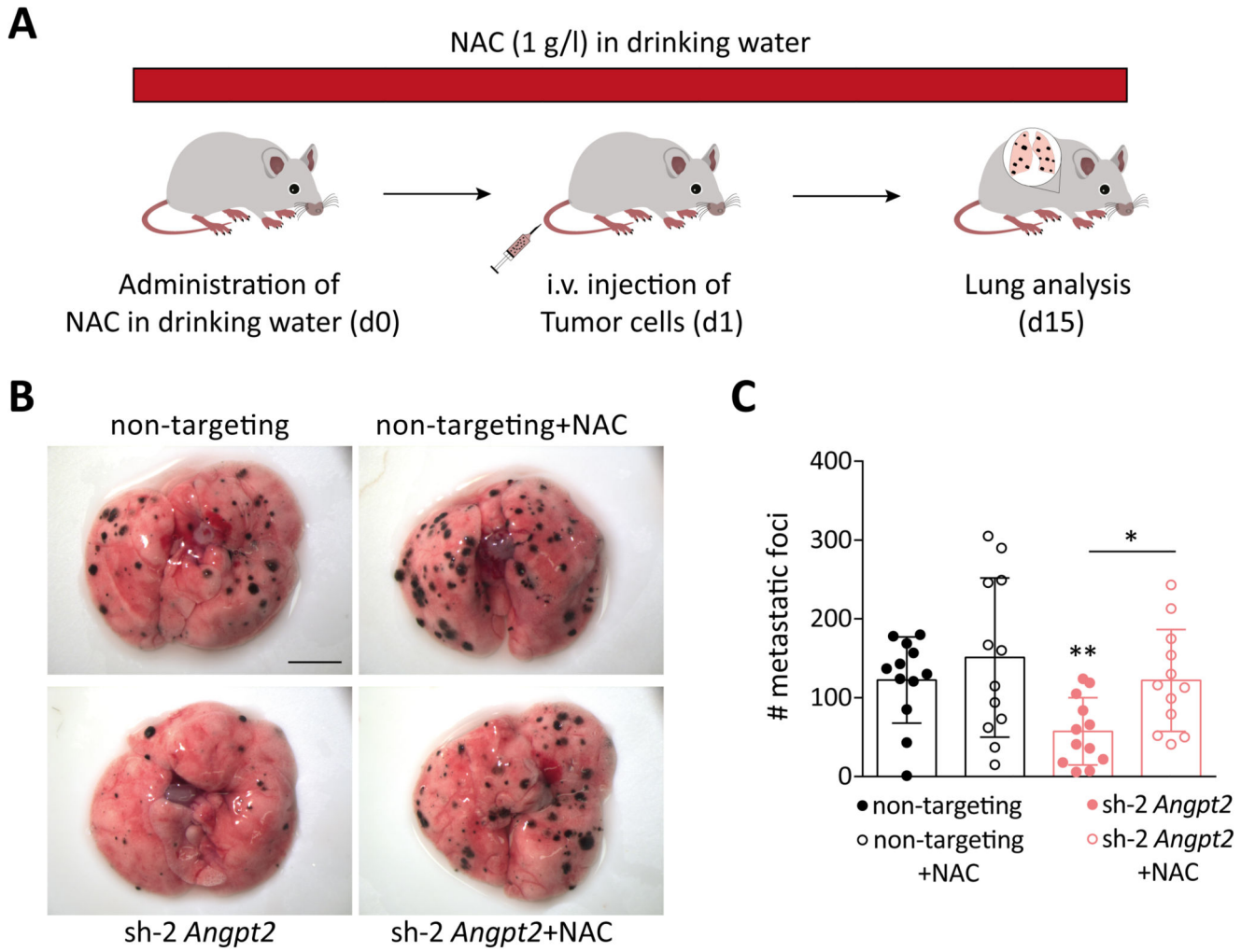


**Figure 6. Administration of NAC rescues metastasis.**

**(A)** Schematic illustration of the rescue experiment to investigate the influence of ROS on regulating tumor cell-*Angpt2* mediated metastasis. **(B)** Control or *Angpt2*-deficient RET cells were injected into the tail vein of C57BL/6N mice. Mice were administered either regular water or water containing 1g/l NAC. Mice were sacrificed after 14 days. Shown are the representative images of lung metastatic foci imaged under a stereomicroscope. Scale bar: 5mm. **(C)** The graph represents the quantitation of lung metastatic foci (n=12; mean ± SD). *, $p<0.05$, **, $p<0.01$, Mann Whitney U test.